Available online at www.sciencedirect.com
SCIENCE DIRECT
International Journal of Mass Spectrometry 249–250 (2006) 8–13
International Journal of Mass Spectrometry
www.elsevier.com/locate/ijms

Impact formation of endohedral fullerenes at surfaces: Comparing field-free yield measurements with model calculations

Y. Manor, A. Kaplan, A. Bekkerman, B. Tsipinyuk, E. Kolodney *

Department of Chemistry, Technion–Israel Institute of Technology, Technion City, Haifa 32000, Israel

Received 4 January 2006; received in revised form 6 January 2006; accepted 6 January 2006
Available online 3 February 2006

Abstract

Yields of endohedral $Cs@C_{60}^+$ ions were measured under field-free conditions, following the impact of low energy (E_o = 40–200 eV) Cs^+ ions with a near-monolayer C_{60} molecules adsorbed on a gold surface. Under these conditions, we were able to apply model calculations and successfully simulate the experimental results. The simulation was carried out by integrating over calculated $Cs@C_{60}^+$ kinetic energy distributions (KEDs). Combined with former measurements and simulations of the KEDs, we arrive at a full and consistent description of both KEDs and impact energy dependent yields, reflecting the combined formation/ejection/decay dynamics of the $Cs@C_{60}^+$ ion.

Keywords: Endohedral fullerene; Surface collision; Ion impact

1. Introduction

The collisional formation of endohedral fullerenes by implantation of atomic ions into C_{60} molecules is a subject of broad interest and importance [1,2]. While the impact insertion of an atomic ion into an isolated C_{60} in the gas phase was studied in detail [3–15], the analogous process with surface adsorbed C_{60} is much less explored and understood. Campbell, Hertel and co-workers have generated $M@C_{60}^+$ endofullerenes at surfaces by bombarding films of C_{60} on silicon with alkali ions (M = Li, Na, K and Rb) [16,17]. A yield of up to 50% was reported for $Li@C_{60}$ and 2–5% for the heavier atoms [17]. This was demonstrated to be a useful and high yield synthetic approach towards isolation of $Li@C_{60}$ and study of its properties [18,19]. A similar implantation method was applied also using He^+ and Ne^+ ions but with much lower efficiencies (∼0.05%) [20]. It is also interesting to note that a leading candidate for spin quantum computing using endohedral fullerenes, $^{14}N@C_{60}$, was synthesized using collisional implantation of atomic nitrogen ion into C_{60} films [21]. An important potential advantage of the endohedral fullerenes approach in quantum computing is that these species can serve as uniform surface nano-traps for the atomic ion or neutral encoded with the qubit (spin state in this case), thus chemically/electronically isolating and shielding them from environmental interferences on the molecular scale. Ordered surface arrays of endohedral fullerenes can potentially offer a solution to the decoherence and scalability problems of quantum computing devices and were indeed proposed as an alternative route towards the realization of quantum-information processing [22,23]. Unfortunately, a very low efficiency of 10^{-7}–10^{-5} was reported (paramagnetic centers) for the ion impact synthesis of $N@C_{60}$ [21]. Clearly, a better understanding of this intra-cage single ion implantation process is valuable from both the basic and practical points of view.

Recently, we have presented a new approach for studying single ion implantation into surface adsorbed fullerenes [24–26]. We have collided low energy (E_o = 40–200 eV) Cs^+ ions with adsorbed C_{60} molecules on gold and silicon surfaces (near-monolayer coverage) and clearly demonstrated a single collision penetration/ejection event of the so-formed $Cs@C_{60}$ endocomplex. The fullerene molecule is actually being picked up off the surface by the penetrating Cs^+ ion. After penetration, the Cs^+ ion back-scatters inside the (still partially open but gradually closing) carbon cage and is responsible for uplifting the just-formed $Cs@C_{60}$ off the surface. The single collision (sub-ps) time scale for the combined formation/ejection event allows only very partial accommodation to the surface such that the information associated with the dynamics of this reactive collision event is

* Corresponding author. Tel.: +972 4 829 3749; fax: +972 4 829 5703.
E-mail address: eliko@tx.technion.ac.il (E. Kolodney).

1387-3806/$ – see front matter © 2006 Elsevier B.V. All rights reserved.
doi:10.1016/j.ijms.2006.01.001

mostly conserved. This process constitutes a unique type of single collision surface pick-up reactive event (Eley–Rideal type). It can also be considered as a novel secondary ion mass spectrometry (static SIMS) process. The concept can possibly be extended to other surface adsorbed species with internal cavities. So far we have reported yield measurements under (surface) potential-biased conditions (aimed at better extraction and detection of the emitted ions) leading to formation of $Cs@C_{60}^+$ and $Cs@C_{70}^+$ on Au and Si surfaces and KEDs measurements for $Cs@C_{60}^+$ on Au for different impact energies. The KEDs measurements were done under both field-free conditions and field-biased conditions. The field-free mode is the most reliable one for comparing with calculations. Measurements with a potential bias (acceleration) can be distorted in a way that cannot be taken into account due to locally inhomogeneous fields or small collection aperture. Sensitivity to local fields is expected to be especially high near threshold, since in this region the kinetic energy of the outgoing endofullerenes is rather low (below 1 eV). The field-biased measurements were done in order to get information on the point of ionization of the surface emitted endohedrals. This is due to the fact that ionization can take place either at the surface or "on-flight" via thermal electron emission. The measured field-free KEDs were compared to calculated KEDs and good agreement was obtained. However, in order to extend the applicability of the proposed model (tested so far only by comparing with the experimental field-free KEDs) one has to compare the field-free model predictions also with yield measurements. This can be done by integration over calculated $Cs@C_{60}^+$ KEDs as a function of Cs^+ impact energy, E_o. For getting the most reliable measurements and consistency with the KEDs results, we have measured the field-free $Cs@C_{60}^+$ impact energy dependent yields and compared with the model calculations. Here, we report these measurements and the agreement obtained with calculations.

2. Experimental

The experimental setup and procedure were described before [24,26]. Only a brief account of the most relevant details will be given here. The experiments were carried out inside a ultrahigh vacuum chamber (base pressure of 5×10^{-10} Torr). An effusive C_{60} oven was aimed at the surface at 45° with respect to its normal while the Cs^+ ion beam was hitting the surface at 90° to the C_{60} beam axis. A quadrupole mass spectrometer (Extrel MEXM-4000) fitted with a homemade retarding field energy analyzer (RFA, $\Delta E = 0.4$ eV) and situated normal to the surface (between the C_{60} source and Cs^+ ion gun) served for KEDs measurements. A sub(near)-monolayer of C_{60} was grown on a gold surface and maintained under steady state conditions simultaneously with the Cs^+ ion bombardment. The layer growth (C_{60} deposition) and removal ($Cs@C_{60}$ emission and C_{60} sputtering) kinetics were probed using the time-dependence of both $Cs@C_{60}^+$ and C_{60}^+ signal after starting C_{60} deposition (while Cs^+ ion beam is already hitting the surface). The detailed kinetics observed and rate constants derived from both "growth/etching" and "etching only" measurements resulted in C_{60} surface coverage of about 0.7 monolayer. Cs^+ beam currents of 1–10 nA were used. Beam energy was well-defined with a narrow (FWHM) width of $\Delta E \leq 0.5$ eV. The ion beam was tilted 2–3° off axis to enable complete blocking of the effusive Cs atomic component. All measurements reported here were performed under strictly field-free conditions. These conditions were assured along the full flight path of the outgoing endohedrals (both parents and fragments) by proper grounding of all electrodes and the surface. Furthermore, all adjacent metal surfaces were carefully shielded by grounded Ta cages.

3. Results and discussion

3.1. Field-free yield measurements

Relative intensities of the parent $Cs@C_{60}^+$ (subject of this report) and kinetically shifted daughter ions $Cs@C_{60-2n}^+$ ($n = 1$–5) measured under field-free conditions as a function of the Cs^+ ion kinetic energy, are given in Fig. 1. Generally, these field-free yield curves are quite similar in appearance to the field-biased ones reported earlier [24]. The main differences observed for the field-free $Cs@C_{60}^+$ results are a somewhat steeper decay at the high energy range ($E_o > 120$ eV) and a more moderate decay at $E_o \leq 60$ eV. The peak of both curves is at the same value of $E_o = 70 \pm 3$ eV. With respect to the daughter ions the only pronounced difference is the ratio of the $Cs@C_{58}^+$ to $Cs@C_{56}^+$ peak intensities, which is smaller for the field-free mode. All other peak positions are quite similar.

The mass integrated (summed over parent and all daughters) $Cs@C_{60-2n}^+$ ($n = 0$–5) ion signals are presented in Fig. 2. Although we do not address here the endohedral daughter ions signals, it is of interest to compare the integrated yield curve measured in the field-free mode with that measured earlier in the field-biased mode. Due to summation over all kinetically shifted daughter ion intensities the mass integrated intensity should depend rather weakly on kinetic parameters such as experimental time windows and parent vibrational temperature. We find

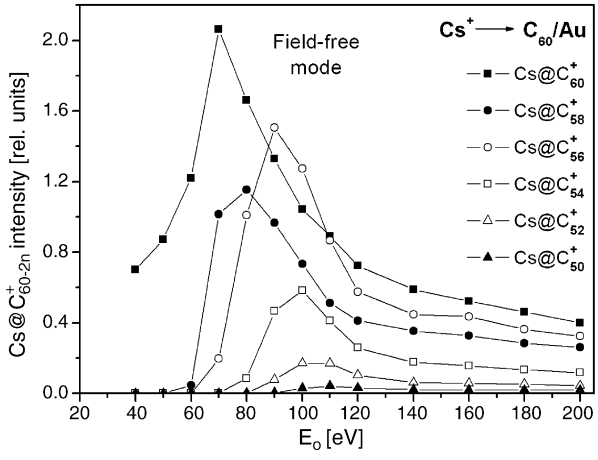

Fig. 1. Relative intensities of the parent endohedral fullerene $Cs@C_{60}^+$ and its daughter ions $Cs@C_{60-2n}^+$ ($n = 1$–5) measured under field-free conditions as a function of the Cs^+ ion energy over the $E_o = 40$–200 range. The substrate is a near-monolayer C_{60} on gold. All ions intensities are normalized to the Cs^+ beam current.

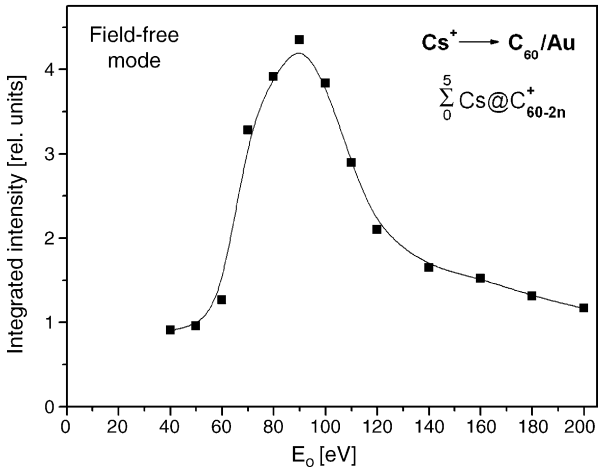

Fig. 2. Integrated $Cs@C^+_{60-2n}$ ($n = 0$–5) ion signal measured under field-free conditions. Each point represents the sum over all ion intensities (parent and fragments), as taken from Fig. 1, down to $Cs@C^+_{50}$.

that the field-free curve is similar in shape and width to the field-biased one but is shifted by about 10 eV to higher E_o values, from a peak value of 80 ± 5 eV for the field-biased curve to 90 ± 5 eV for the field-free one.

3.2. Model calculations and comparison with experiments

Details of the model are given in Ref. [26]. Briefly, the model first describes the formation of the $Cs@C_{60}$ at the surface and its ejection off the surface and then links between the resulting original KEDs (at the surface) and the measured KEDs (at the detector) by taking into account the various competing decay processes which the surface ejected endohedral undergoes during its flight time to the detector. The processes considered are the formation of the $Cs@C_{60}$ at the surface following penetration by the Cs^+ ion, its ejection off the surface with a certain kinetic energy $E^{@}$ (after overcoming its adsorption energy to the surface $E^{@}_{ad}$) and its thermal decay kinetics during flight. The first part of the model (formation/ejection dynamics) leads to a strong correlation between the vibrational and the kinetic energy $E^{@}$ of the outgoing $Cs@C_{60}$. The faster endohedrals are also hotter. This interesting feature eventually leads to preferential depletion of the high energy tail of the $Cs@C^+_{60}$ KEDs due to fragmentation. Since the E_o dependent yield curve for $Cs@C^+_{60}$ will be calculated by integrating over the corresponding KED at a given E_o value, one should first present the simulation of the KEDs and extent of agreement with experiment. As the full calculation was already presented before [26], here we will give just the different dependencies controlling the calculated KEDs. The interested reader is referred to the original discussion for details. After penetrating the C_{60} cage (mass M) by breaking n carbon–carbon bonds, the Cs^+ ion (mass m), while inside the cage, backscatters with kinetic energy $E^{Cs}_{scat.} = (E_o - nE_b)K$ with E_b as the average C–C bond energy and $(1 - K)$ as the kinetic energy loss coefficient. The spread in K values is taken to be described by a Gaussian distribution centered around some K_o value with a width parameter δ. The density of the probability distribution $P(E^{@},E_o)$ for emitted neutral endohedrals with kinetic energy $E^{@}$ can therefore be shown to be:

$$P(E^{@}, E_o) = \frac{1}{\delta \cdot [E^{@}_o(E_o) + E^{@}_{ds}]\sqrt{2\pi}} \times \exp\left[-\frac{1}{2}\frac{[E^{@} - E^{@}_o(E_o)]^2}{\delta^2 \cdot [E^{@}_o(E_o) + E^{@}_{ds}]^2}\right] \quad (1)$$

where

$$E^{@}_o(E_o) + E^{@}_{ds} = (E_o - nE_b)K_o\frac{m}{m+M} \quad (2)$$

and

$$E^{@} + E^{@}_{ds} \le (E_o - nE_b)\frac{m}{m+M}. \quad (3)$$

In order to take into account the outgoing particle flux variation (per unit solid angle) one has to assume a specific barrier function $B(E^{@}, E^{@}_{ds})$ which depends on the field of attractive surface forces acting on the particle. One usually distinguishes between the two limits of a "flat barrier" that leads to a refractive-like behavior along the outgoing trajectory [27,28] and a "spherical barrier" which results in no angular flux variation namely $B(E^{@}, E^{@}_{ds}) \equiv 1$ [28]. We have found that the spherical barrier assumption is in better agreement with the experimental KEDs and it will therefore be used in the yield simulation as well. The third function that has to be taken into account is the probability Φ that after penetrating the C_{60} cage the Cs^+ ion will remain trapped and will not break out. This probability function was shown to be:

$$\Phi(E^{@}) = \frac{m}{M}\frac{nE_b}{E^{@} + E^{@}_{ds}} \quad (4)$$

for $E^{@} > (m/M) \cdot nE_b - E^{@}_{ds}$ and $\Phi(E^{@}) = 1$ otherwise.

Finally, the decay kinetics of the emitted $Cs@C_{60}$ is described in terms of Klots finite heat bath theory [29]. These processes include the fragmentation and delayed ionization of the neutral parent $Cs@C_{60}$ emitted from the surface and the fragmentation of the $Cs@C^+_{60}$ ions (formed by thermionic ionization of the neutral). All this information is included in the so-called differential breakdown function $f(E^{@},g)$ where g represents the part of the energy nE_b (released upon cage closure) that is converted to $Cs@C_{60}$ internal energy, while its complementary part $(1 - g)$ is dissipated into the surface. In the calculation, we will assume that all $Cs@C_{60}$ are leaving the surface as neutrals and thermionically ionize on flight. This assumption is also supported by experiment [26]. The $f(E^{@},g)$ function takes into account the complex decay kinetics including radiative cooling following the power law: $k_{rad} = 4.5 \times 10^{-17} T^6$ eV s^{-1} (Ref. [30]). In order to follow the derivation of this function one is referred to the appendix of Ref. [26] where the "decay process related" isokinetic temperatures are derived. The final form of the $f(E^{@},g)$ function calculated within the relevant detection time windows is also given in Ref. [26]. We further assume that the factor g can be described by a Gaussian distribution $G(g,g_o)$ centered around some g_o value with width parameter δ_g such that the integrated

breakdown curve $F(E^{@})$ takes the form:

$$F(E^{@}) = \int_0^1 G(g, g_o, \delta_g) f(E^{@}, g) \mathrm{d}g. \quad (5)$$

The shape of the KEDs detected at the output of the mass spectrometer should therefore be:

$$\frac{\mathrm{d}N(E^{@}, E_o)}{\mathrm{d}E^{@}} = P(E^{@}, E_o) \cdot \Phi(E^{@}) B(E^{@}, E_{ds}^{@}) F(E^{@}). \quad (6)$$

A comparison between experimental and calculated $Cs@C_{60}^{+}$ KEDs for two values of Cs^{+} impact energies E_o is presented in Fig. 3. The following four adjustable parameters were fitted in the calculation: $K_o = 0.4$, $\delta = 0.5$, $g_o = 0.85$, $\delta_g = 0.2$. The penetration threshold nE_b was taken as 20 eV (3–5 carbon–carbon bonds). All other values required for the calculation are given and discussed in Ref. [26]. The calculation is carried out for "delayed ionization only" and spherical barrier ($B(E^{@}, E_{ds}^{@}) = 1$) assumption. As can be seen in Fig. 3, good agreement was obtained between the model calculation and experiment. It was found that the KEDs are mainly sensitive to the g_o, δ_g parameters ($G(g,g_o)$ distribution) and are only weakly controlled by the K_o and δ values ($P(E^{@},E_o)$ distribution). In order to test the validity of the "delayed ionization only" assumption we have repeated the calculation under the "surface ionization only" assumption. In this case, it was not possible at all to reproduce the peak-shape behavior of the KEDs. Only monotonously decaying KEDs could be obtained. These results strongly support the assumption that the large majority of the ionization events are thermally delayed.

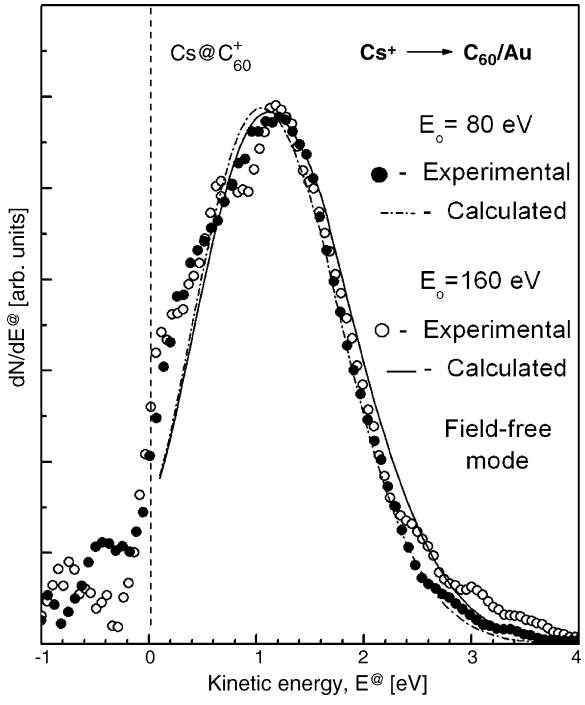

Fig. 3. A comparison between experimental (solid and empty circles) and calculated (dashed and solid line) $Cs@C_{60}^{+}$ KEDs following Cs^{+} ion impact with $E_o = 80$ and 160 eV. The calculation is carried out for spherical barrier and "delayed ionization only" (see text for explanation). Radiative cooling is taken into account.

The E_o dependent yield of $Cs@C_{60}^{+}$ ions can now be calculated by integrating Eq. (6) over $E^{@}$:

$$Y(E_o) = \left(1 - \frac{E_o^{pen}}{E_o}\right) \int_0^{E_{max}^{@}(E_o)} P(E^{@}, E_o) \cdot \Phi(E^{@}) B(E^{@}, E_{ds}^{@}) F(E^{@}) \mathrm{d}E^{@}. \quad (7)$$

The pre-integral function represents the threshold behavior of the E_o dependent probability for Cs^{+} penetration into the C_{60} cage. A linear threshold law for the excess of impact energy E_o just above the threshold value for penetration E_o^{pen} was assumed. This can be compared with the function $1 - \Phi(E^{@})$ from Eq. (4) which gives the probability of the Cs^{+} ion to escape out of the cage (frustrated implantation event). We will use $E_o^{pen} = nE_b$ in accordance with our model for the $Cs@C_{60}$ formation at the surface. The condition $E^{@} + E_{ds}^{@} = (E_o - nE_b)m/(m/M)$ (see Eq. (3)) defines the maximum energy $E_{max}^{@}(E_o)$ (upper integral limit) in the kinetic energy distribution of the escaping $Cs@C_{60}$ just after leaving the surface. Once we set $E^{@} = 0$ in the above condition we get the Cs^{+} impact energy threshold E_o^{thr} for the yield $Y(E_o)$:

$$E_o^{thr} = E_{ds}^{@} \frac{m + M}{m} + nE_b. \quad (8)$$

Please note that $E_o^{thr} > E_o^{pen}$.

Measured and calculated $Y(E_o)$ dependences (Eq. (6)) are presented in Figs. 4 and 5. The same (numerical) values of all model parameters used for calculating the KEDs (both the four parameters $K_o = 0.4$, $\delta = 0.5$, $g_o = 0.85$, $\delta_g = 0.2$ and all other given values) were used also for calculating $Y(E_o)$. The calculation was carried out using the assumption of a spherical barrier. Note that the intensities ratio between the calculated (with radiative cooling) and measured curves was arbitrarily adjusted for best fit with the high energy side ($E_o \geq 70$ eV). The ratio

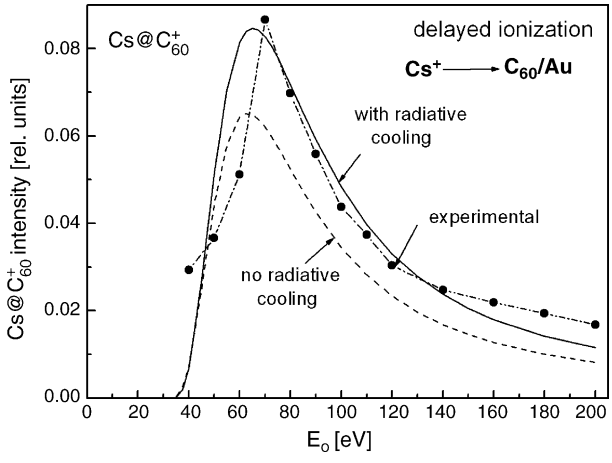

Fig. 4. A comparison between experimental (solid circles, taken from Fig. 1) and calculated (solid and dashed lines) yield curves for $Cs@C_{60}^{+}$. The intensities ratio between the calculated (with radiative cooling) and experimental curves was arbitrarily set for best fit with the high energy side of the experimental yield curve ($E_o > 70$ eV). The calculation is carried out under the assumption of "delayed ionization only" with and without radiative cooling.

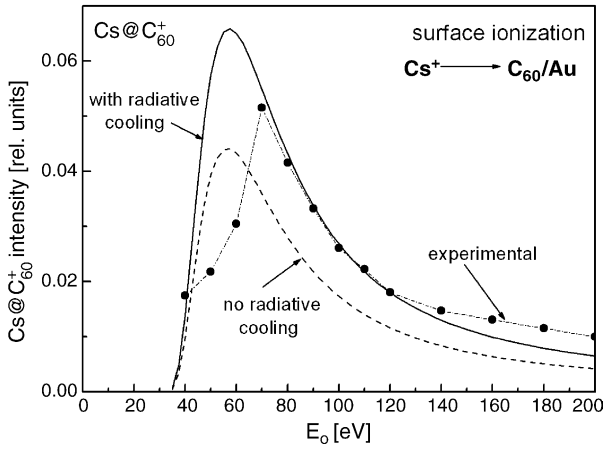

Fig. 5. A comparison between experimental (solid circles, taken from Fig. 1) and calculated (solid and dashed lines) yield curves for $Cs@C_{60}^{+}$. The intensities ratio between the calculated (with radiative cooling) and experimental curves was arbitrarily set for best fit with the high energy side of the experimental yield curve ($E_o > 70$ eV). The calculation is carried out under the assumption of "surface ionization only" with and without radiative cooling.

between the calculated curve with radiative cooling (solid line) and without radiative cooling (dashed line) is determined by the calculation.

The agreement between experiment and calculation within the "delayed ionization only" assumption is presented in Fig. 4. Both peak shape and decay at the high energy side are reasonably reproduced but agreement is worse at the low energy side and threshold region. The calculated maximum of the curve (with radiative cooling) is at 65 eV while the experimental value is at 70 eV. The experimental curve appears to be narrower than the calculated one and the near threshold behavior is not well reproduced. Due to the unique condition of $E_o^{thr} > E_o^{pen}$ and the importance of the field-free threshold behavior it will be interesting to further explore this issue. Based on experimental evidence and the clear disagreement with the calculated KEDs shape, the possibility of surface ionization as an important ionization process in this experiment, was already ruled out. However, in order to find out whether there is an agreement with the yield measurements, we have repeated the calculation under the "surface ionization only" assumption and the results are presented in Fig. 5. As can be seen, the peak behavior is roughly reproduced but agreement with experiment in terms of shape and maximum value is worse than for the "delayed ionization only" calculations (maximum yield at about 56 eV as compared with the experimental 70 eV value). It is clear that the integral (yield) measurements constitutes a much less sensitive test for the validity of these assumptions (regarding the ionization mode) than the differential (KEDs) measurements.

4. Summary

We have measured the yields of endohedral $Cs@C_{60}^{+}$ and its $Cs@C_{60-2n}^{+}$ ($n = 1$–5) daughter ions, under field-free conditions, following the impact implantation of Cs^{+} ions into C_{60} molecules adsorbed on a gold surface. The surface coverage is slightly below monolayer. The penetration/ejection is a single collision event where the impact implanted Cs^{+} ion is backscattered inside the cage thus leading to the up-lifting of the just-formed $Cs@C_{60}$ off the surface. This actually constitutes direct pick-up (Eley–Rideal type) of the fullerene cage. Formerly we have shown that model calculations can reproduce quite well the field-free kinetic energy distributions of the outgoing endohedrals. Here, we apply the same model to the field-free yield measurements by integrating over the calculated (impact energy dependent) kinetic energy distributions. We show that using this model with a single set of four adjustable parameters we can reproduce the main features of both the impact energy dependent yield curves and kinetic energy distributions.

Acknowledgements

This research was supported by a grant from the Israel Science Foundation and by the James Frank Program.

References

[1] M.S. Dresselhaus, G. Dresselhaus, P.C. Eklund, Science of Fullerenes and Carbon Nanotubes, Academic Press, San Diego, CA, 1996.
[2] H. Shinohara, Rep. Prog. Phys. 63 (2000) 843.
[3] T. Weiske, D.K. Bohme, J. Hrusak, W. Kratschmer, H. Schwarz, Angew. Chem. Int. Ed. Engl. 30 (1991) 884.
[4] T. Weiske, H. Schwarz, D.E. Giblin, M.L. Gross, Chem. Phys. Lett. 227 (1994) 87.
[5] E.E.B. Campbell, R. Ehlich, A. Hielscher, J.M.A. Frazo, I.V. Hertel, Z. Phys. D At. Mol. Clusters 23 (1992) 1.
[6] R. Kleiser, H. Sprang, S. Furrer, E.E.B. Campbell, Z. Phys. D At. Mol. Clusters 28 (1993) 89.
[7] Z. Wan, J.F. Christian, S.L. Anderson, Phys. Rev. Lett. 69 (1992) 1352.
[8] Z. Wan, J.F. Christian, Y. Basir, S.L. Andreson, J. Chem. Phys. 99 (1993) 5858.
[9] J.F. Christian, Z. Wan, S.L. Andreson, J. Chem. Phys. 99 (1993) 3468.
[10] Y. Basir, S.L. Andreson, J. Chem. Phys. 107 (1997) 8370.
[11] R.C. Mowrey, M.M. Ross, J.H. Callahan, J. Phys. Chem. 96 (1992) 4755.
[12] R. Ehlich, E.E.B. Campbell, O. Knospe, R. Schmidt, Z. Phys. D At. Mol. Clusters 28 (1993) 153.
[13] R. Ehlich, O. Knospe, R. Schmidt, J. Phys. B At. Mol. Phys. 30 (1997) 5429.
[14] V. Bernshtein, I. Oref, J. Chem. Phys. 109 (1998) 9811.
[15] K. Ohno, Y. Maruyama, K. Esfarjani, Y. Kawazoe, N. Sato, R. Hatakeyama, T. Hirata, M. Niwano, Phys. Rev. Lett. 76 (1996) 3590.
[16] R. Tellgmann, N. Krawez, S.H. Lin, I.V. Hertel, E.E.B. Campbell, Nature 382 (1996) 407.
[17] E.E.B. Campbell, R. Tellgmann, N. Krawez, I.V. Hertel, J. Phys. Chem. Solids 58 (1997) 1763.
[18] V.N. Popok, I.I. Azarko, A.V. Gromov, M. Jönsson, A. Lassesson, E.E.B. Campbell, Solid State Commun. 133 (2005) 499 (and references therein).
[19] F. Rohmund, A.V. Bulgakov, M. Hedén, A. Lassesson, E.E.B. Campbell, Chem. Phys. Lett. 323 (2000) 173.
[20] R. Shimshi, R.J. Cross, M. Saunders, J. Am. Chem. Soc. 119 (1997) 1163.
[21] T. Almeida Murphy, Th. Pawlik, A. Weidinger, M. Höhne, R. Alcala, J.-M. Spaeth, Phys. Rev. Lett. 77 (1075–1078) (1996) 1075.
[22] J. Twamley, Phys. Rev. A 67 (2003) 052318.
[23] W. Harneit, Phys. Rev. A 65 (2002) 032322.

[24] A. Kaplan, A. Bekkerman, B. Tsipinyuk, E. Kolodney, J. Chem. Phys. 117 (2002) 3484.
[25] A. Kaplan, Y. Manor, A. Bekkerman, B. Tsipinyuk, E. Kolodney, Int. J. Mass. Spectrom. 228 (2003) 1055.
[26] A. Kaplan, Y. Manor, A. Bekkerman, B. Tsipinyuk, E. Kolodney, J. Chem. Phys. 120 (2004) 1572.
[27] M.W. Thompson, Philos. Magn. 18 (1968) 377.
[28] A. Budrevich, B. Tsipinyuk, A. Bekkerman, E. Kolodney, J. Chem. Phys. 106 (1997) 5771.
[29] (a) C.E. Klots, J. Chem. Phys. 90 (1989) 4470;
(b) C.E. Klots, Z. Phys. D At. Mol. Clusters 22 (1991) 335.
[30] S. Tomita, J.V. Andersen, C. Gottrup, P. Hvelplund, U.V. Pedersen, Phys. Rev. Lett. 87 (2001) 073401.